High performance Pirani vacuum gauge

JinShown Shie, Bruce C. S. Chou, and YeongMaw Chen

Citation: Journal of Vacuum Science & Technology A **13**, 2972 (1995); doi: 10.1116/1.579623
View online: http://dx.doi.org/10.1116/1.579623
View Table of Contents: http://scitation.aip.org/content/avs/journal/jvsta/13/6?ver=pdfcov
Published by the AVS: Science & Technology of Materials, Interfaces, and Processing

High performance Pirani vacuum gauge

Jin-Shown Shie, Bruce C. S. Chou, and Yeong-Maw Chen
Institute of Electro-Optical Engineering, National Chiao Tung University, Hsinchu Taiwan, Republic of China

(Received 23 February 1995; accepted 17 July 1995)

As an extension of previous work in our laboratory, a wide-range Pirani gauge that is capable of measuring vacuum pressure down to 10^{-7} Torr reproducibly has been built. The micromachined Pirani sensor used in the experiments has a suspended membrane that is supported by the nearly radiation-limited, thermally insulating beam leads crossing over a V-groove cavity. A method of partial dummy compensation, as proposed previously by Weng and Shie for eliminating the ambient drift, is proved here to be very effective with a thermal drift as small as only 5.7 μV/°C. It has also been found that a thermal-stress-induced piezoresistive effect, which has a profound influence on the limitation of measurement, appears in the constant-bias operation wherein the sensor temperature rises with the reduction of gas pressure and therefore thermal conduction. This effect causes the irreproducibility of pressure measurements by the device below 10^{-5} Torr. In addition to its inherently higher sensitivity, a constant-temperature circuit together with a thermoelectric stabilization of the sensor substrate temperature can eliminate the induced piezoresistive error. The constant-temperature circuit operating on the micro-Pirani sensor together with the above-mentioned temperature compensation and the stabilization methods have extended gauge capability down to 10^{-7} Torr, which is only limited by the signal readout resolution ($\sim$1 μV). This is three orders of magnitude more sensitive than the conventional vacuum gauges of the thermal conductivity type. © *1995 American Vacuum Society.*

I. INTRODUCTION

Ever since the invention of the Pirani gauge in 1906,[1] the gauge has been widely used but limited only to the vacuum pressure range from 10^{-4} to 100 Torr. As a thermal-conductivity-type vacuum sensor, this gauge is based on the principle that the heat loss of a hot object to the ambient depends on the pressure of the surrounding gas. The vacuum pressure, therefore, can be calculated according to the heat loss variation which manifests itself by a temperature change on a thermally sensitive physical parameter associated with the hot object.

The conventional thermal-based vacuum gauge is bulky and laborious in fabrication. New structures using monolithic micromachining technology that have the advantage of batch productivity have been developed recently.[2–8] These include the Pirani type of floating-polysilicon bridge developed by Robinson *et al.*[2] and Mastrangelo and Muller[3] and the thermopile type developed by van Herwaarden and Sarro.[4–7] However, the lowest pressure measured by their studies were limited to only 1 mTorr, owing to immature structure design and sensitivity-improving techniques. Recently, Weng and Shie[8] have been able to make a micro-Pirani sensor capable of measuring pressure to 0.1 mTorr or lower. The structure of the sensor, however, is not yet optimized.

To extend the previous work[8] the authors have continued to construct a highly sensitive Pirani vacuum gauge which has overcome problems that previously existed. This gauge is capable of detecting the pressure down to 10^{-7} Torr, as will be described in detail in the following.

II. SYSTEM CONFIGURATION

As shown in Fig. 1, the Pirani vacuum gauge that we have built has a micromachined sensor attached to a thermoelectric cooling stage. The device itself contains an on-substrate dummy resistor for ambient temperature compensation that will be described later. The temperature of the stage is sensed by a thermistor and stabilized within 23 ± 0.001 °C by a thermostat with proportional integral-phase lead feedback control to further nullify the ambient drift effect.[9] The Pirani sensor is driven either by a constant-bias (CB) or by a constant-temperature (CT) circuit. The output signals of the circuits are acquired by a digital voltmeter (DVM), which is sampled and recorded by a PC through GPIB interface connected to the voltmeter. The sensor stage is installed inside a vacuum chamber to be pumped for the experiment. The pumping system contains a mechanical pump, a turbopump, and an ion pump. The nitrogen gas source is linked through a needle valve into the chamber for adjustments of pressure which are monitored by a set of Pirani and cold-cathode gauges.

III. THE FABRICATED SENSOR AND ITS CHARACTERISTICS

A. Device structure

Figure 2 shows a scanning electron microscopy (SEM) picture of the fabricated micromachined Pirani sensor. It contains an active sensor element (R_s) on a floating glass membrane and an on-substrate dummy sensor element (R_d) for temperature compensation purposes, these are fabricated simultaneously onto (100) silicon wafer. The floating membrane (5000 Å thermal oxide) is supported by the thermally insulating leads crossing over the corners of the etched V-groove cavity. The serpentine resistors of the Pt film (1500 Å), both for the active and for the dummy sensors, are coated on the thermal oxide with Cr film (50 Å) as the buffer layer.

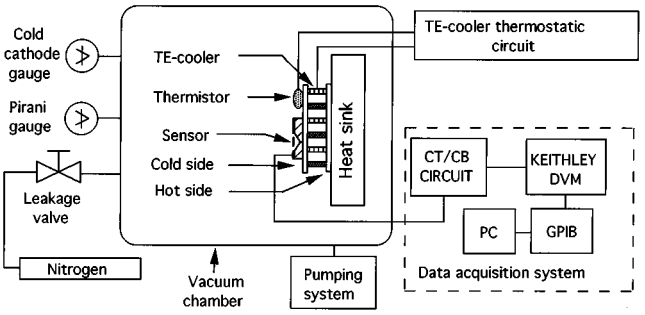

FIG. 1. System configuration used for the experiments.

The temperature coefficient of resistance (TCR) of the film formed is typically 0.28%/°C by this process. The devices are passivated by atmospheric pressure chemical vapor deposition (APCVD) phosphosilicate glass (PSG) (6000 Å) before the last step of anisotropic etching for V-groove formation. The sensor has a cavity of 325 μm square each edge (C), a lead width of 5.7 μm (A), and a lead length of 110 μm (B).

The advantage of this device structure to the beam bridge[2,3] is that heat loss to the substrate is limited by the beam leads. Therefore, the temperature on the membrane area can be considered to be homogeneous.

B. Thermal characteristics

In direct current (dc) steady state, the input power to the micro-Pirani sensor is equal to the heat loss rate according to the energy conservation, namely,

$$G(T-T_a)=V^2/R_s=IV, \tag{1}$$

where T_a is the ambient temperature, V^2/R_s is the electrical bias power on the sensor R_s, and V is the corresponding voltage drop. The total heat-loss conductance, G, is contributed by three conduction mechanisms, the radiative (G_r), the gaseous (G_g), and the solid (G_s).

The first radiative mechanism can be derived according to the Stefan–Boltzmann law as

$$G_r=2\epsilon\sigma A_s(T^2+T_a^2)(T+T_a). \tag{2}$$

Here σ is the Stephen–Boltzmann constant, ϵ the emissivity, T and T_a are the temperatures of the floating plate and the ambient, respectively, and A_s is the sensor active area.

The second mechanism of gaseous thermal conduction according to the early work of Dushman[8,10]

$$G_g=\kappa P\left(\frac{P_{tl}}{P+P_{tl}}+\frac{P_{tu}}{P+P_{tu}}\right),$$

$$\kappa=\frac{\varphi}{2-\varphi}G_a A_s, \tag{3}$$

$$G_a=\Lambda_0\left(\frac{273.2}{T_a}\right)^{1/2}.$$

φ is the accommodation coefficient of gas; G_a and Λ_0 are the free molecular conductivities at ambient temperature and at 0 °C, respectively; P is the gas pressure; P_{tl} and P_{tu} are the transition pressures on the lower and the upper sides of the floating membrane, which are inversely proportional to the effective separations of the membrane to the heat sinks,[10] respectively. Physically, the transition pressure denotes the separation of the viscous state from the molecular state in gaseous conduction.

To the solid conduction G_s of the fabricated device, since heat flow is limited by the beam lead parts, an empirical formula can be adopted as[8]

$$G_s=\left[\frac{1}{4.2kd}\left(\frac{B}{A}\right)+5\times10^4\right]^{-1}, \tag{4}$$

where k is the thermal conductivity of the leads and d is its effective thickness averaged over the minor oxide contribution. The last number in the equation is the spreading resistance close to the lead ends.

Figure 3 shows the numerical calculation of the fabricated device according to these equations. A transition pressure of 2.3 Torr is shown. This value is determined by the effective separations on both sides of the floating membrane. In this sensor, the predominant one is the distance from the membrane to the V-groove surface. An equivalent distance of 0.18 C is obtained from a three-dimensional numerical calculation of gas flux[8] by assuming a flat plane instead of the V-shaped surface. Furthermore, the total conductance is reduced to a constant value, equal to the sum of G_s and G_r when the pressure approaches absolute vacuum.

We also can evaluate the total conductance experimentally according to the relationship of Eq. (1), wherein the temperature rise, $T-T_a$, is measured from the resistance value of the sensor Pt film, which is

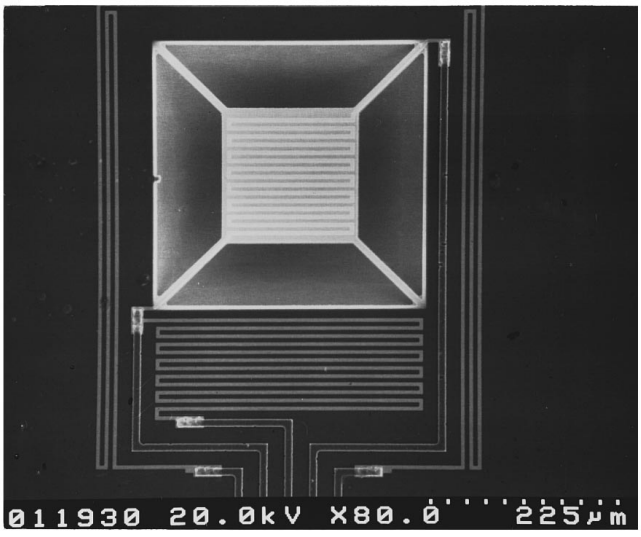

FIG. 2. SEM picture of the fabricated micro-Pirani sensor (R_s=600 Ω) with the associated dummy sensor (R_d=900 Ω).

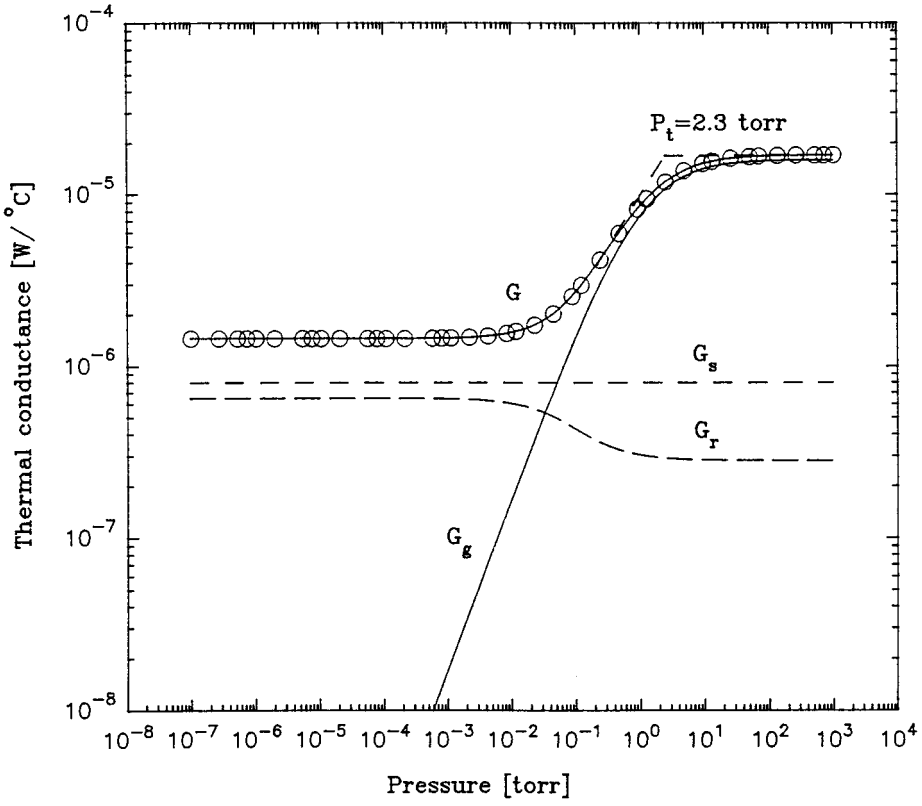

FIG. 3. Numerical calculations (lines) and experimental measurements (circles) of the thermal conductance of the device with 1.5 V constant bias voltage.

$$R_s = R_a[1+\alpha_a(T-T_a)]; \tag{5}$$

here R_a and α_a are the resistance and TCR of the active sensor at T_a, respectively. The experimental result evaluated accordingly shows agreement to the numerical calculations indicated by the circles in Fig. 3. This fact ensures the authenticity of Eqs. (2)–(4).

One can observe in Fig. 3 that the conductance approaches saturation when the pressure is larger than the transition pressure around 2.3 Torr, dominated by the viscous state of the gas conduction. Below the transition pressure, wherein is the molecular state, the total conductance as well as G_g decrease linearly with the pressure. When the pressure is around 0.1 Torr, the gas conduction becomes comparable to G_s+G_r and deviation from linearity appears in the total conductance. Evidently, this device structure has an extremely low solid conductance, less than 1×10^{-6} W/°C, which is comparable to G_r. Excellent resolvable pressure is thus achievable by this nearly radiation-limited solid conductance, as will be clear from the following. Incidentally, for the CB mode of Fig. 3, the radiative conduction, G_r, increases in the low pressure region because of the membrane temperature rise associated with the falling of gaseous conduction.

IV. SENSING CIRCUITS AND RESPONSES

Both constant-bias and constant-temperature circuits are used for the experiments. The performance of these two circuits on the micro-Pirani sensor was analyzed in detail by Weng and Shie in their previous report.[8] A more complete analysis is condensed as follows.

For the dc steady state of the CB Wheatstone bridge circuit shown in Fig. 4(a), a voltage difference related to vacuum pressure is delivered after calibration nulled by the following relationship[8]

$$\begin{aligned} V_s(\mathrm{CB}) &= KV_b\left[\left(\frac{(T-T_a)}{(T_c-T_a)}\frac{R_{sc}}{R_s}\frac{G}{G_s+G_r}\right)^{1/2}-1\right], \\ &= KV_b\left[\left(\frac{(T-T_a)}{(T_c-T_a)}\frac{1+\alpha_a(T_c-T_a)}{1+\alpha_a(T-T_a)}\frac{G}{G_s+G_r}\right)^{1/2}-1\right], \\ &= KV_b\left[\left(\Gamma(T)\,\frac{G}{G_s+G_r}\right)^{1/2}-1\right], \end{aligned} \tag{6}$$

with

$$\begin{aligned} K &= \frac{R_4}{R_{sc}+R_4}=\frac{R_2}{R_1+R_2}, \\ \Gamma &= \frac{(T-T_a)}{(T_c-T_a)}\,\frac{1+\alpha_a(T_c-T_a)}{1+\alpha_a(T-T_a)}. \end{aligned} \tag{7}$$

Here V_b is the bias voltage and $(1-K)V_b$ the voltage drop on the sensor, R_{sc} is the sensor resistance at the calibrated reference temperature, T_c, namely, at the calibrated reference pressure, absolute vacuum.

In the low pressure regime, the gaseous conduction is small compared to G_s+G_r, thus Eq. (6) reduces to

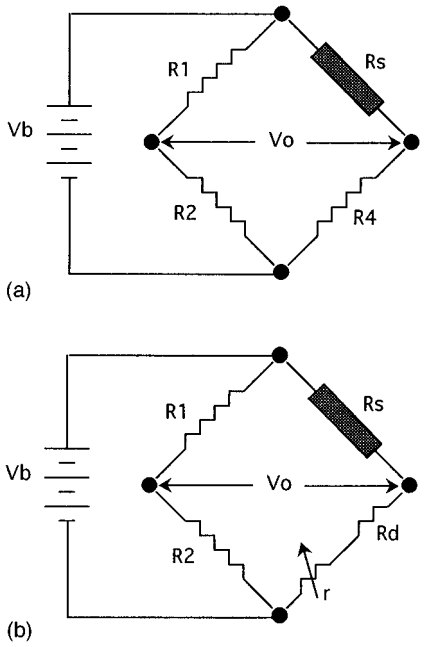

FIG. 4. (a) Conventional Wheatstone bridge circuit for Pirani gauge. R_s is the active sensor. (b) Schematic diagram of the partial compensation method for a constant-bias circuit. R_d is the dummy resistor of R_s material and r is a temperature-independent constant resistor.

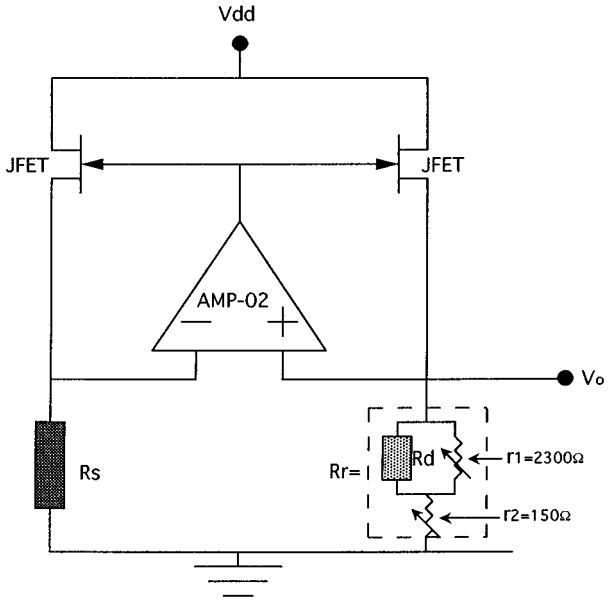

FIG. 5. The CT circuit used in this experiment. R_r is the reference resistor. The partial compensation method is employed here in a slightly complicated configuration. r_1 and r_2 are both adjustable to obtain the best compensation.

$$V_s(\mathrm{CB}) = KV_b\left[\Gamma^{1/2}\left(1+\frac{G_g}{G_s+G_r}\right)^{1/2}-1\right]$$

$$\cong \frac{KV_b}{(G_s+G_r)}\,\kappa\Gamma^{1/2}P = S_{\mathrm{CB}}P, \tag{8}$$

the gauge sensitivity,

$$S_{\mathrm{CB}} \equiv \frac{KV_b}{(G_s+G_r)}\,\kappa\Gamma^{1/2}. \tag{9}$$

Note that, when the pressure approaches absolute vacuum, the sensor temperature $T=T_c$, and $\Gamma(T)\cong\Gamma(T_c)=1$.

When the pressure approaches infinity, the gaseous conduction is dominant and saturated. The signal becomes

$$V_s(\mathrm{CB}) \cong KV_b\left[\left(\frac{\Gamma_\infty \kappa P_t}{G_s+G_r}\right)^{1/2}-1\right] \tag{10}$$

with $P_t = P_{\mathrm{tl}} + P_{\mathrm{tu}}$.

For CT operation,[11–13] the Mastrangelo and Muller circuit,[3] as shown in Fig. 5 is adopted for the experiment, except that a matching pair of the *n*-channel junction field effect transistor (JFET) in saturation mode are used instead of the metal–oxide semiconductor FET (MOSFET) as the voltage-controlled current sources. This circuit was thoroughly studied by Mastrangelo.[14] In its operation, the instrumentation amplifier (AMP-02) forces the voltage on R_s sensor tracking to that of R_r reference. And, owing to the matching condition of the JFET pair, this results in $R_s \cong R_r$ (or $T\cong T_c$), namely, the quasiconstant-resistance (or -temperature) state on the sensor.

For CT static operation, one obtains from Eq. (1) the following relationships:

$$G(T_c-T_a) = V_o^2/R_s,$$

$$(G_s+G_r)(T_c-T_a) = V_{oc}^2/R_{sc} = V_{oc}^2/R_s;$$

here

$$V_s(\mathrm{CT}) = V_o - V_{oc}, = [(T_c-T_a)R_s(G_s+G_r)]^{1/2}$$

$$\times\left[\left(\frac{G}{G_s+G_r}\right)^{1/2}-1\right], \tag{11}$$

$$= V_{oc}\left[\left(\frac{G}{G_s+G_r}\right)^{1/2}-1\right].$$

Following the same arguments as in the CB circuit, one gets

$$V_s(\mathrm{CT}) \cong \frac{V_{oc}}{(G_s+G_r)}\,\kappa P, \quad P\to 0,$$

$$= S_{\mathrm{CT}}P \tag{12}$$

$$V_s(\mathrm{CT}) \cong V_{oc}\left[\left(\frac{\kappa P_t}{G_s+G_r}\right)^{1/2}-1\right], \quad P\to\infty, \tag{13}$$

where V_{oc} is the voltage read on the sensor at the calibrated conditions as $(1-K)V_b$ in the CB mode. Comparing Eqs. (8) and (12), one knows that, if $KV_b = V_{oc}$, the two circuits have the same sensitivities close to absolute vacuum and both are inversely proportional to the residual conductance, G_s+G_s. However, the CB sensitivity, S_{CB}, is lower at higher pressure due to the Γ factor, whereas S_{CT} remains constant. Also, both are proportional to the active sensor area. Close-form dynamic analysis of this circuit, however, is difficult owing to its complicated feedback characteristics.

V. TEMPERATURE COMPENSATION AND STABILIZATION

A. Partial compensation method

As analyzed by previous authors,[8] the minimum detectable pressure of the Pirani gauge is limited by the system noise, the dc-offset nulling accuracy for eliminating the effect of G_s+G_r, and the ambient temperature drift on the device signal. In general, the first two factors can be solved by the use of low-noise circuitry and a high precision potentiometer. However, the last factor of voltage drift caused by the ambient temperature fluctuation is more difficult to eliminate than the other two.

In the conventional Pirani-type gauge, the effect of ambient drift is compensated by an identical dummy tube. However, this compensation effect has so far only reached a sensing limit of 10^{-3} Torr due to the difficult device matching. This is because conventional Pirani tubes are produced one at a time and therefore an identical dummy is not possible. In addition, bulky conventional tubes are impossible to situate in identical environments. These problems can be solved if microelectronic technology is utilized for the fabrication of both the active and the dummy sensors.

As mentioned earlier when discussing Weng and Shie's work,[8,15] a new ambient temperature compensation method can be adopted. This method as shown in Fig. 4(b), utilizing a partial dummy compensation that uses a combination of a temperature-independent constant resistor, r, and a temperature-dependent dummy resistor R_d for the R_4 bridge arm. R_d has the same material as R_s and is fabricated simultaneously on the silicon substrate without V-groove cavity underneath it, as was shown previously in Fig. 2. However, since the thermal resistances to the substrate of R_s and R_d are different, they do not have the same temperature as well as the TCR, according to Eq. (5), under bias condition. Hence the complete elimination of thermal drift is not possible here with a sole dummy sensor like conventional types. The idea of partial dummy compensation described above thus can improve TCR matching. Following the previous analysis, which was not proved experimentally, the ambient temperature effect can possibly be reorganized for the CB mode in the form of

$$\frac{dV_s}{dT_a}=\frac{V_b R_s R_d \alpha_a}{(R_s+R_d)^2}\,\frac{\{\alpha_a(T-T_a)-\beta[1+\alpha_a(T-T_a)]\}}{[1+\alpha_a(T-T_a)]}. \tag{14}$$

Here β is called the compensation factor and defined as $\beta=r/(r+R_d)$, $\beta=0$ is the full compensation, while $\beta=1$ the uncompensation. The temperature drift can be eliminated completely by setting $dV_s/dT_a=0$ in Eq. (14), which gives

$$\beta=\frac{\alpha_a(T-T_a)}{1+\alpha_a(T-T_a)}. \tag{15}$$

This condition is partially true for the CB mode since T varies with the degree of measured vacuum, but the compensation is most important for the high vacuum regime where the signal is small and the sensor temperature is nearly constant. However, for the CT mode, the condition of Eq. (15) would be completely true if the partial compensation method is equally effective for it.

To prove the method experimentally, the device with 1 V bias was placed in an oven whose temperature was set from 30 to 100 °C. The membrane temperature was measured about 35 °C above that of the oven. The results of the measurement are depicted in Fig. 6, where the uncompensated one shows a drift of -56.7 mV, while the fully compensated one shifts only 4.2 mV for the temperature range. The new partially compensated method drifts, however, only 0.4 mV, or equivalently 5.7 μV/°C. This is a 142 time improvement over the uncompensated and 11 times over the fully compensated. In our measurement, β is set to a value of 0.037, a value close to the theoretical estimation of 0.08 calculated from Eq. (15). The difference probably resulted from the small nonconstancy to the temperature of resistor r.

To test its effectiveness, the partial compensation method is also adopted in the CT circuit for experiment without theoretical analysis. The result is depicted in Fig. 6. It shows that it is equally applicable to the CT circuit of Fig. 5. Here the configuration of the partial compensation is more complicate than that of the CB circuit.

B. Substrate temperature stabilization

As stated before, the gaseous thermal conductance is inversely proportional to the heat transport distance between the hot membrane and the heat sink. The very small spacing between the substrate and the membrane, namely, the V-groove region, makes its role in gaseous conductance much greater than that of the upper part. Hence the sensor temperature is floated with that of the substrate instead of the ambient if the two temperatures are different. Control of the substrate under constant temperature conditions thus can further stabilize the device from the influence of ambient temperature.

To control the substrate temperature in constancy, we have employed a feedback-controlled thermoelectrical (TE) cooling method. The thermostat was made by sealing the sensor chip on a TE cooling stage where an attached thermistor is used to sense the temperature of the stage. The sensed temperature is fed back to a control circuit by proportional-integral-phase lead to achieve a cooled temperature at 23 ± 0.001 °C for long-term stability.[9] An accurate model of the thermostat transfer function has been carefully studied for parametric adjustments. This stable temperature in addition to the partial compensation method should give an extremely low thermal drift voltage of 5.7 nV to the CB operation according to Fig. 6. This voltage level is far below the lowest reading resolution (1 μV) of the DVM, thus not the limiting factor to detection resolution.

VI. EXPERIMENTS AND RESULTS

A. Experimental procedures

The procedures to acquire experimental data follow the steps as below.

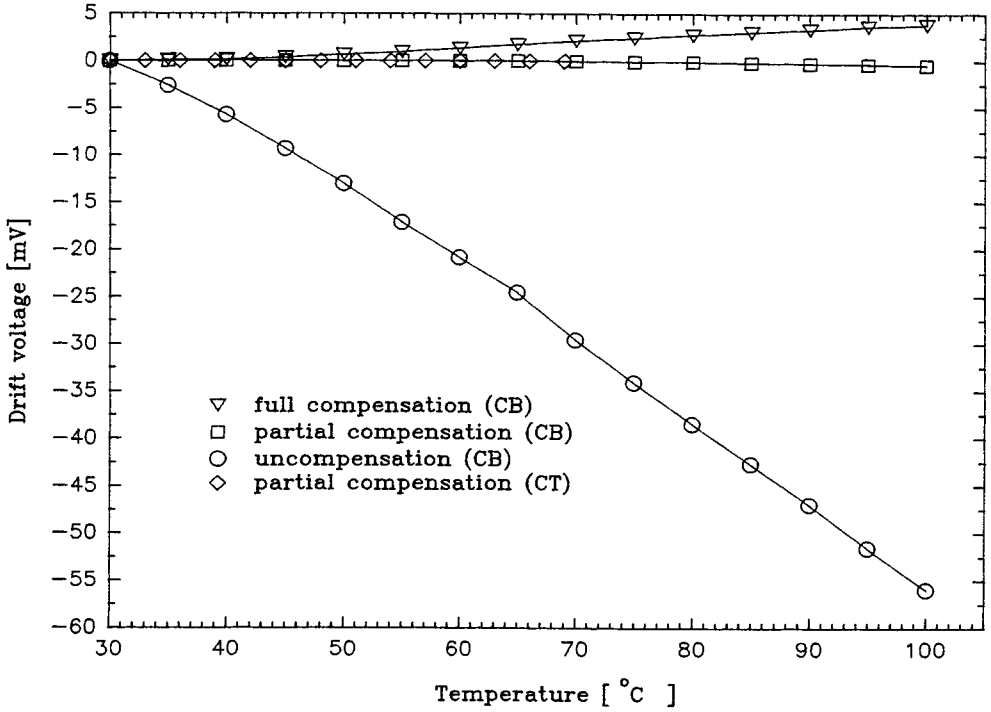

FIG. 6. Experimental measurements of different compensation conditions. Notice that the drift is only 5.7 μV/°C for the partial compensation in the CB mode with β=0.037.

(1) Install the device with a thermostat stage into the chamber and evacuate the system down to its lowest achievable vacuum of 1×10^{-8} Torr.

(2) Set the pressure at the pseudoabsolute vacuum for calibration reference and nullify as accurately as possible the output voltages [V_o in Figs. 4(b) and 5] of the circuits to eliminate the offset voltage induced by G_s, G_r, and other causes.

(3) Adjust the needle valve to have the nitrogen gas flow in to the desired pressure to be measured; this is monitored by the Pirani gauge or by the cold-cathode gauge shown in Fig. 1.

(4) Read the voltage from the circuits by the DVM and transmit them to the PC through the GPIB interface. In the lower pressure region, 100 sampling data are accumulated and averaged for each 10 s period. The sampling rate and the period can be faster or shorter in the high pressure regime where signals are large.

B. Results

Figure 7 shows the measured results of the CB operation. The solid line is the theoretical calculation according to Eq. (6). One can observe the close agreement between theory and the experiment, and can also see deviation from the theoretical calculation starts as early as 10^{-4} Torr, which is same as in the previous report.[8] We think the cause can be attributed to the large variation of the membrane temperature to the gas pressure in the CB mode, which was measured to be from 60 to 360 °C in the pressure range. This makes the compensation factor, β, difficult to be determined correctly. Another cause is from the smaller signal output of the CB circuit that limits the reading resolution. It is also found from Fig. 7 that the measured signal voltages appear to be different between the upward and the downward pressure trends. The authors believe this is caused by the residual thermal stress existing in the glass membrane in the pressure cycle. The thermal stress induces a piezoresistive effect on the platinum film. This induced stress, which is caused by the moisture-absorbing effect of PSG, is also evidenced in other works[16,17] in studying VLSI processes.

Operation with a CT circuit will induce only constant thermal stress in the sensor, which can be nulled out at the starting period. Hence the circuit can be utilized to prove the above hypothesis and overcome the problems.

Figure 8 shows the result of the CT measurements. The theoretical calculation uses the same parameters adopted for CB. The residual signal due to the presumed thermal-stress-induced piezoresistive effect disappears, and the reproducible measurements can be further lowered to 1×10^{-7} Torr. This low detectable pressure was never reported before by other workers using a Pirani vacuum gauge. The measurement is limited by the DVM reading resolution of 1 μV. This voltage level corresponds to a resistance change in the sensor of several mΩ only. It is worth noting that, in such a situation, any vibration reaching the gauge must be reduced to a minimal extent to avoid noises induced during the lowest pressure measurements.

Both electrical signals are saturated above certain high pressure turning points which are solvable by equating Eqs. (8) and (10) for CB, and Eqs. (12) and (13) for CT,

$$\frac{KV_b}{(G_s+G_r)}\,\kappa P = KV_b\left[\left(\frac{\Gamma_\infty \kappa P_t}{G_s+G_r}\right)^{1/2}-1\right], \tag{16}$$

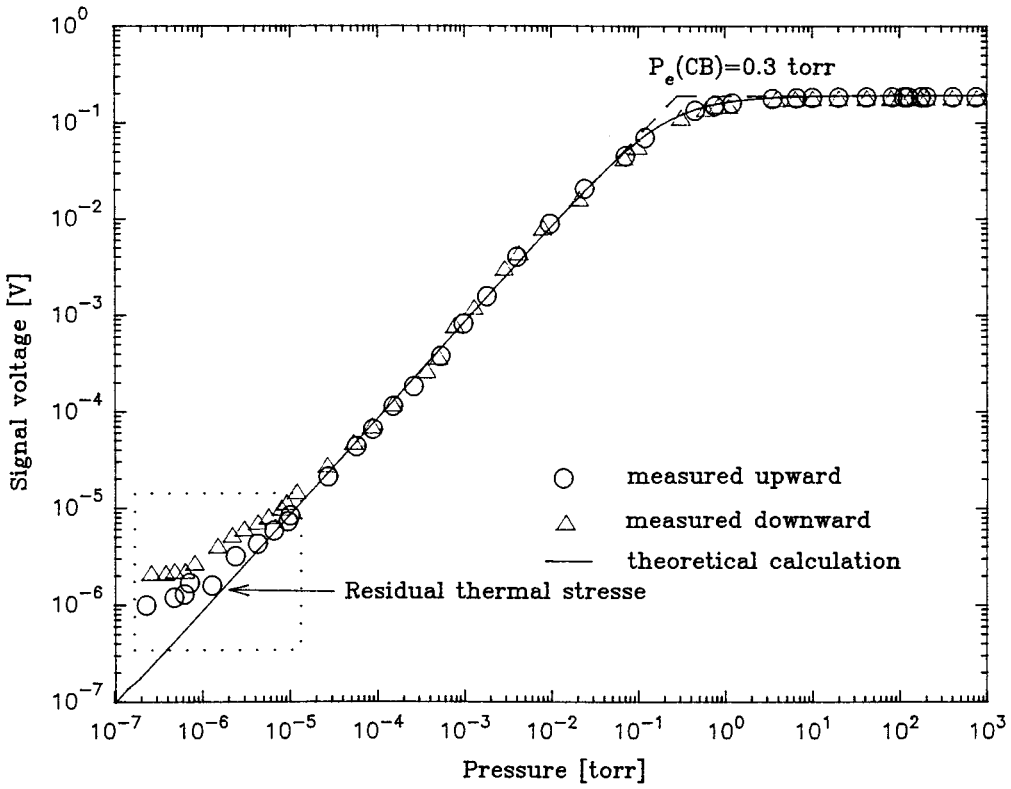

FIG. 7. Signal voltage as a function of pressure for the CB circuit. (○): Upward pressure; (△): downward pressure. Note the existence of a residual signal between the two sets of measurements at low pressure below 3×10^{-5} Torr. The solid line is the theoretical calculation according to Eq. (6).

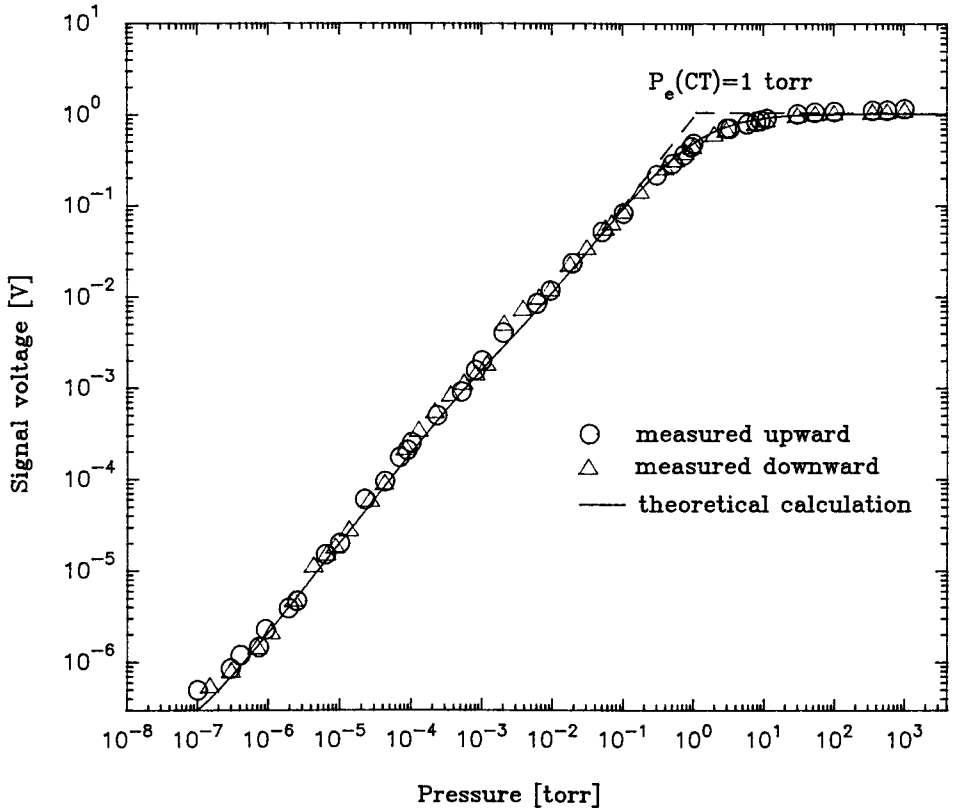

FIG. 8. Signal voltage as a function of pressure for the CT circuit. (○): Upward pressure; (△): downward pressure. Consistency between the two sets of measurements is observed. One can see that the lowest detectable pressure, 10^{-7} Torr, is obtained, limited by the DVM reading ability of 1 μV.

$$\frac{V_{oc}}{(G_s+G_r)}\,\kappa P = V_{oc}\left[\left(\frac{\kappa P_t}{G_s+G_r}\right)^{1/2}-1\right]. \tag{17}$$

The results are definable as the electrical transition pressure, P_e, with

$$P_e(\mathrm{CB})=\left(\frac{(G_s+G_r)\Gamma_\infty P_t}{\kappa}\right)^{1/2}-\frac{(G_s+G_r)}{\kappa}, \tag{18}$$

$$P_e(\mathrm{CT})=\left(\frac{(G_s+G_r)P_t}{\kappa}\right)^{1/2}-\frac{(G_s+G_r)}{\kappa}. \tag{19}$$

Further derivation shows the relationship

$$\frac{P_e(\mathrm{CB})+(G_s+G_r)/\kappa}{P_e(\mathrm{CT})+(G_s+G_r)/\kappa}=\Gamma_\infty^{1/2}<1. \tag{20}$$

The CT operation therefore, possesses a wider measurable pressure range. For practical values of this device, $\Gamma_\infty \cong 1/9$ and $(G_s+G_r)/\kappa \cong 10^{-4}$ which is small compared to P_e. Hence, P_e(CT) is about three times larger than P_e(CB). This is consistent with experiments shown in Figs. 7 and 8.

VII. CONCLUSIONS

A highly sensitive micro-Pirani sensor has been fabricated that is capable of measuring pressure linearly from 1 down to 10^{-7} Torr. The gauge employs the partial compensation method with an on-substrate dummy sensor made by semiconductor fabrication. The dummy structure has the advantage of matching with the active sensor. Additionally, a thermostat to stabilize the temperature of the sensor substrate on a TE cooling stage has been developed to further reduce thermal drift.

It has been discovered that the constant-temperature circuit has the advantages of exempting the thermal-stress effect and a better adjustment of the temperature compensation factor β, in addition to higher sensitivity.

In the experiments, the lowest pressure measurable has been limited by the capability of DVM and its nulling accuracy. It is imaginable that, if device structure can be further optimized for higher sensitivity, then the potential to achieve 10^{-9} Torr resolution is possible.

ACKNOWLEDGMENTS

The authors wish to express their appreciation to U. C. Chang for assistance in building the thermostat in the experiments, and to Opto Tech Corporation in Science Based Industry Park of Hsinchu, Taiwan, for partial technical support of device processing. This project was supported by the National Science Council of the Republic of China under project Contract No. NSC-82-0404-E-009-127.

[1]M. Pirani, Verh. Dtsch. Phys. Ges. **8**, 686 (1906).
[2]A. M. Robinson, P. Haswell, R. P. Lawson, and M. Parameswaran, Rev. Sci. Instrum. **63**, 2026 (1992).
[3]C. H. Mastrangelo and R. S. Muller, IEEE J. Solid-State Circuits **26**, 1998 (1991).
[4]A. W. Van Herwaarden and P. M. Sarro, Sensors and Actuators **8**, 187 (1985).
[5]A. W. Van Herwaarden and P. M. Sarro, J. Vac. Sci. Technol. A **5**, 2454 (1987).
[6]A. W. Van Herwaarden and P. M. Sarro, J. Phys. E **21**, 1162 (1988).
[7]A. W. Van Herwaarden and P. M. Sarro, Sensors and Actuators **14**, 259 (1988).
[8]P. K. Weng and J. S. Shie, Rev. Sci. Instrum. **65**, 492 (1994).
[9]U. C. Chang, M.E. thesis, National Chiao Tung University, Republic of China, 1993.
[10]S. Dushman, *Scientific Foundations of Vacuum Technique*, 2nd ed. (Wiley, New York, 1962).
[11]P. Freymuth, Rev. Sci. Instrum. **38**, 677 (1967).
[12]P. Freymuth, J. Phys. E: Sci. Instrum. **11**, 915 (1978).
[13]J. F. Kreider, IEEE Trans. Instrum. Meas. June, 190 (1973).
[14]Mastrangelo, Ph.D. thesis, UC Berkeley, 1991.
[15]J. S. Shie and P. K. Weng, U.S. Patent No. 5,347,869 (1994).
[16]S. H. Sun, M.E. thesis, National Chiao Tung University, Republic of China, 1993.
[17]T. H. T. Wu and R. S. Rosler, Solid State Technol. **36**, 65 (1992).